Zhao et al. *Microsystems & Nanoengineering* (2026)12:65
https://doi.org/10.1038/s41378-026-01193-5

Microsystems & Nanoengineering
www.nature.com/micronano

ARTICLE Open Access

Robotic cell transportation system based on micropipette resistance modeling

Qili Zhao[1,2], Mengya Liu[1,2], Ripeng Zhu[1,2], Jinyu Qiu[1,2], Shaojie Fu[1,2], Ruimin Li[1,2] and Xin Zhao[1,2]✉

Abstract

Cell transportation, using a micropipette to pick and place cells from one droplet to another, is a key step in many cell engineering applications. However, most of the current cell transportation operations rely on microscope vision guidance, unsuitable for the future integrated and automated cell engineering applications where microscopic views are usually missed. The presenting microscopic view-free cell transportation systems are only applicable for special giant cells due to the bilayer structure of operation micropipettes. In this paper, a robotic cell transportation system based on micropipette resistance modeling was developed to transport common-sized cells without a microscopic view. First, a narrow-necked micropipette (NNM) was fabricated for holding the target cell inside the micropipette during transportation. Then, a gap resistance model, an aspiration resistance model, and an injection resistance model of the micropipette were developed to land on the cell plane, pick and release the cell without a microscopic view, respectively. Based on the above work, a robotic transportation process was established to transport the common-sized cells without a microscopic view. Finally, experimental results demonstrate that the proposed system can land on the cell plane with 100% success rate. It can transport 10 μm-level sized HeLa cells and 100 μm-level sized porcine oocytes with efficiencies comparable to common microscopic view-based methods and without harm to cell survival rate. Our microscopic cell transportation system can be upgraded to a high-throughput version for integrated automated cell engineering applications in the future.

Introduction

Cell transportation, pick-and-place the target cells from one place to another with a micropipette, is a key step in cell engineering applications such as nuclear transplantation[1,2], embryo vitrification[3,4], cell culturing process[5], cell manipulation and measurement[6,7]. The cell transportation process is schematically shown in Fig. 1. The operator usually uses a common straight micropipette to land on the petri dish bottom where the cells stay, aspirate one cell into the micropipette, position it at a location close to the micropipette opening through aspiration pressure adjustment, move to another droplet and release the cell with a positive pressure pulse[4]. The above cell transportation tasks usually need to be performed under microscopic view to obtain the positions of cells and micropipettes. However, there are still many cell engineering applications where microscopic views are not available while cell transportation tasks are still desired. For example, in-box cell culturing and operation devices[3,8,9] are key equipment for future integrated and automated cell engineering applications. Integration of the microscope inside them is a challenging task due to the narrow space inside them (see Fig. 1b). However, these cell transportations are still requisite for medium change for suspended cells, such as animal oocytes/embryos in these devices. Besides, for some cells stained by fluorescent dyes, over-exposure of them under bright field may lead to photobleaching issues[10,11], which may cause extra difficulties in the observation of the target cells after transportation. Thus, the transportation of these stained cells under dark conditions without a microscopic view is preferred to prevent photobleaching issues. For the above

Correspondence: Xin Zhao (zhaoxin@nankai.edu.cn)
[1]National Key Laboratory of Intelligent Tracking and Forecasting for Infectious Diseases, Engineering Research Center of Trusted Behavior Intelligence, Ministry of Education, Tianjin Key Laboratory of Intelligent Robotic (tjKLIR), Institute of Robotics and Automatic Information System (IRAIS), Nankai University, Tianjin 300350, China
[2]Institute of Intelligence Technology and Robotic Systems, Shenzhen Research Institute of Nankai University, Shenzhen 518083, China

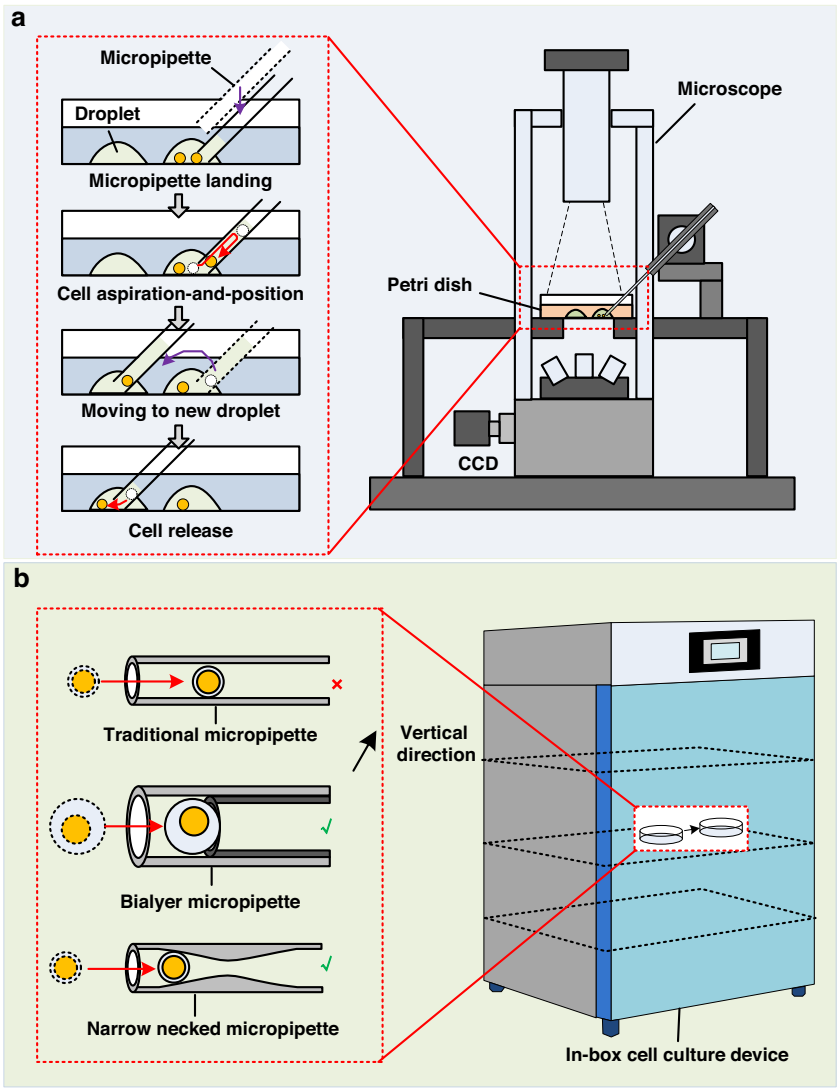

Fig. 1 Schematics: cell transportation for cell engineering applications. a Traditional cell transportation procedures and system setup. **b** Micropipettes used in microscopic view-free cell transportation for in box cell engineering applications

applications, the microscopic view-free cell transportation systems are highly desired.

In recent years, automated cell transportation system research has made significant progress. For example, Zhang et al. proposed a single sperm aspirating and positioning technique inside a micropipette and achieved closed-loop robust control of sperm dynamics[12]. Shan et al. considered the compressibility and deformation of oil and proposed a cell aspiration model based on an oil-driven pump, then designed an adaptive controller for cell positioning[9]. Zhao et al. used an extended state observer (ESO)-backstepping controller to control cell movement for precise cell positioning in a micropipette[13]. Sun et al. realized precise aspiration and positioning of microbeads based on the dynamics of spherical cells inside and outside the micropipette[14]. Zhang et al. modeled the dynamics of embryo motion and developed a linear quadratic regulator controller to pick multiple embryos one by one into the micropipette for embryo vitrification[15]. However, the micropipettes utilized in these systems are still the common straight micropipettes with constant inner diameters. Due to the lack of structure in the common micropipette to quickly stop and hold the aspirated cell by force (as shown in Fig. 1b), the cell positioning inside the micropipette needs to be realized by repeatably adjustment of aspiration pressure through microscopic view-based cell motion control methods. The microfluidic devices have been designed to conduct cell holding and solution exchange tasks inside microfluidic chips[16–18]. In comparison to traditional cell

transportation methods, these devices can save some microscopic visual-based steps, such as cell positioning and the travel of cells from old droplets to new droplets. However, the target cell picking and solution exchange tasks still need to be performed under microscopic view feedback. Relying on a microscopic view limits the applications of the above automated cell transportation systems in future integrated in-box cell engineering applications.

From the above analysis, a new micropipette with a special structure to stop and hold the cell by force is required to transport the cell without microscopic view feedback. Using a common straight micropipette with an opening size smaller than the cell size can hold the cell at its opening[16,19], and thereby, saving the cell positioning and holding problems. However, in that way, part of the cell membrane will be exposed outside when the micropipette passes through the space between two droplets. As the space among droplets is usually an oil and air environment, the exposed cell membrane may be dissolved or oxidized by oil or the air[20]. To protect the cell and meanwhile solve the positioning and holding tasks, the cell is preferred to be stopped and held inside the micropipette during transportation. To achieve this, a new narrow-necked micropipette (NNM), with a larger opening to aspirate cells in and a small inner diameter inside the micropipette to hold the cell, is required for transporting cells. In previous research, we have assembled a bilayer micropipette by inserting a thinner glass tube into a thicker one from behind[21]. The bilayer micropipette can aspirate the cell into the larger opening of the outer thick tube and hold the cell with the smaller opening of the inside thin tube, as shown in Fig. 1b. However, due to their small diameter (hundreds of microns) and relatively long length (centimeter size), the crush between the two micropipettes easily occurs during the assembling process, which easily breaks the two glass tubes. At present, only a thick enough bilayer micropipette with an inner diameter of 1 mm and an outer diameter of 1.5 mm was successfully assembled for transporting 1-mm-level-sized giant cells, such as zebrafish embryos, in our previous research. For the common-sized cells, such as 100-μm-level-sized domestic oocytes and 10 μm-level-sized somatic cells, a new thin, narrow-necked micropipette needs to be designed and fabricated.

Even with appropriate narrow-necked micropipettes suitable for small cells, key steps in cell transportation, such as landing on the petri dish bottom, picking, and releasing the cell, still need to be realized without a microscopic view. With a microscopic view, the landing task can be realized through first autofocusing of the cell and then lowering the micropipette to the focal plane of the cell[22]. As the cells usually stay at the bottom of the petri dish, Wang et al. introduce a contact detection method between the micropipette tip and the petri dish bottom based on the prolongation of the tip after it contacts the bottom[23]. Unfortunately, the prolongation detection still relies on a microscopic view. The compressing force on the bottom exerted by the micropipette tip can be utilized to judge the contact between them without a microscopic view[21]. However, when the micropipette tip becomes thinner, the contact force decreases significantly and may become too slight to be detected due to the resolution limitation of microforce sensors. Further, lowering down the tip, although it can increase the contact force, may also increase breaking incidence possibility of the thin micropipette tip. Addressing this, a noncontact landing detection of the micropipette tip to the petri dish bottom is required to prevent the breakage of the thin micropipette tip.

Besides the landing detection, the holding and release detections also need to be realized without microscopic view feedback. In time holding detection can stop further aspiration pressure increase, which may cause further mechanical harm to cell by the squeezing of the narrow neck after cell holding. Realtime release detection can prevent too much medium being released into the new droplet, reducing the contamination incidences in the new droplet. When the cell is held and released by the micropipette, the variation speed changes of pressure inside micropipette resulting from the blockage and reopening of the gas channel have been utilized to judge the holding and release[21]. However, the above pressure variation speed changes are positively correlated with the opening size of the micropipette. In previous study, we found that when the inner diameter of the micropipette is less than 300 μm, the above pressure variation speed changes become too weak to be detected by commercial pressure sensors[21,24,25]. For the thinner micropipettes for transportation of common cells with diameter less than 300 μm, new detection methods of cell holding and release are still required for microscopic view of free cell transportation. The detailed summary of the related research work is presented in Table 1.

In this paper, a robotic cell transportation system was developed to transport common-sized cells without a microscopic view. First, an NNM was fabricated through a heating and rotating method to hold the cell inside the micropipette during transportation. Then, a gap resistance model of the tilting NNM approaching the petri dish bottom was developed to guide the former to land on the latter without microscopic view feedback. Further, an aspiration resistance model of the NNM was developed to hold and release the cell without microscopic view feedback. Based on the above work, a robotic micropipette resistance-guided transportation process was developed for transporting common-sized cells without a microscopic view. Experimental results demonstrate that the

Table 1 The detailed summary of the related research work

Methods	Reference[9]	Reference[12]	Reference[13]	Reference[14]	Reference[15]	Reference[16–18]	reference[21]	This paper
Key technologies	Cell aspiration model	Single sperm aspirating and positioning	ESO backstepping controller	Precise microbead aspiration positioning	Embryo dynamics modeling, LQR controller	Microfluidic	Pressure variation model	Resistance modeling
Micropipette	Straight micropipettes	Straight micropipettes	Straight micropipettes	Straight micropipettes	Straight micropipette	Microfluidic chips	Bilayer micropipette	NNM
Advantages	High adaptability in the aspiration process	Robust control of sperm motility	High precision cell location	Precise location of microbeads/spherical cells	Multiple embryo operations	Less reliance on vision	Giant cell transportation without vision	Non-visual precision transportation
Drawbacks	Rely on view feedback	Rely on view feedback	Rely on view feedback	Rely on view feedback	Rely on view feedback	Rely on view feedback	Micropipettes are subject to breakage	Complex micropipette fabrication

proposed system can land on the petri dish bottom with a 100% success rate. It can transport 10-μm-level sized HeLa cells and 100-μm-level sized porcine oocytes with efficiencies comparable to traditional microscopic view-based methods. The viability testing results demonstrate no harm to the cell survival rate of our system. Our microscopic cell transportation system can be upgraded to a microfluidic version, which is able to perform high-throughput cell transportation for integrated and automated cell engineering applications in the future.

Materials and methods

Narrow-necked micropipette (NNM) design and fabrication for robotic transportation of common-sized cells

As shown in Fig. 2a, to fabricate an NNM from a common straight micropipette, three key geometrical parameters of NNM include the inner radius at the micropipette opening D_O, inner radius at the narrow neck position D_N and the distance between the micropipette opening and narrow neck position d_{ON}.

The value of D_O should be larger than the target cell size in order to aspirate the latter in. However, the large D_O may cause too long a time and too much energy to generate a narrow neck inside a micropipette, which needs to be smaller than the size of the target cell. Through a large number of tests, the inner diameter of the micropipette opening is set as 1.2-folded cell diameter to aspirate the cell into it.

For the inner radius of the narrow neck D_N, on one hand, it should be large enough to generate a large enough aspiration pressure to aspirate the target cell into the micropipette opening. On the other hand, a too large D_N may fail to hold the cell at the narrow neck position. The maximum value of D_N is determined by the maximum aspiration pressure and the size of target cell according to our previous study. The detailed determination process of D_N has been provided in Section 1 of the Supplementary file.

Furthermore, the liquid stored between the micropipette opening and the narrow neck position will be injected into the new droplet during the release of the cell. Therefore, a too large d_{ON} increases the amount of liquid introduced to the new droplet from old droplet in cell transportation, increasing the contamination rate in new droplet. Meanwhile, a too-small d_{ON} could not provide enough space to save the cell body during the cell transportation. According to fabrication results using our commercial microforge equipping a glass heating ball with a 250 μm diameter, the length of the generated narrow neck section is usually about 2–3 folded D_O to transport 10-μm-sized somatic cells. For NNMs to transport 100 μm-sized oocytes, the length of the narrow neck section is about 2–3 folded D_O. Considering the above points, the d_{ON} of NNMs for 10 μm-sized somatic

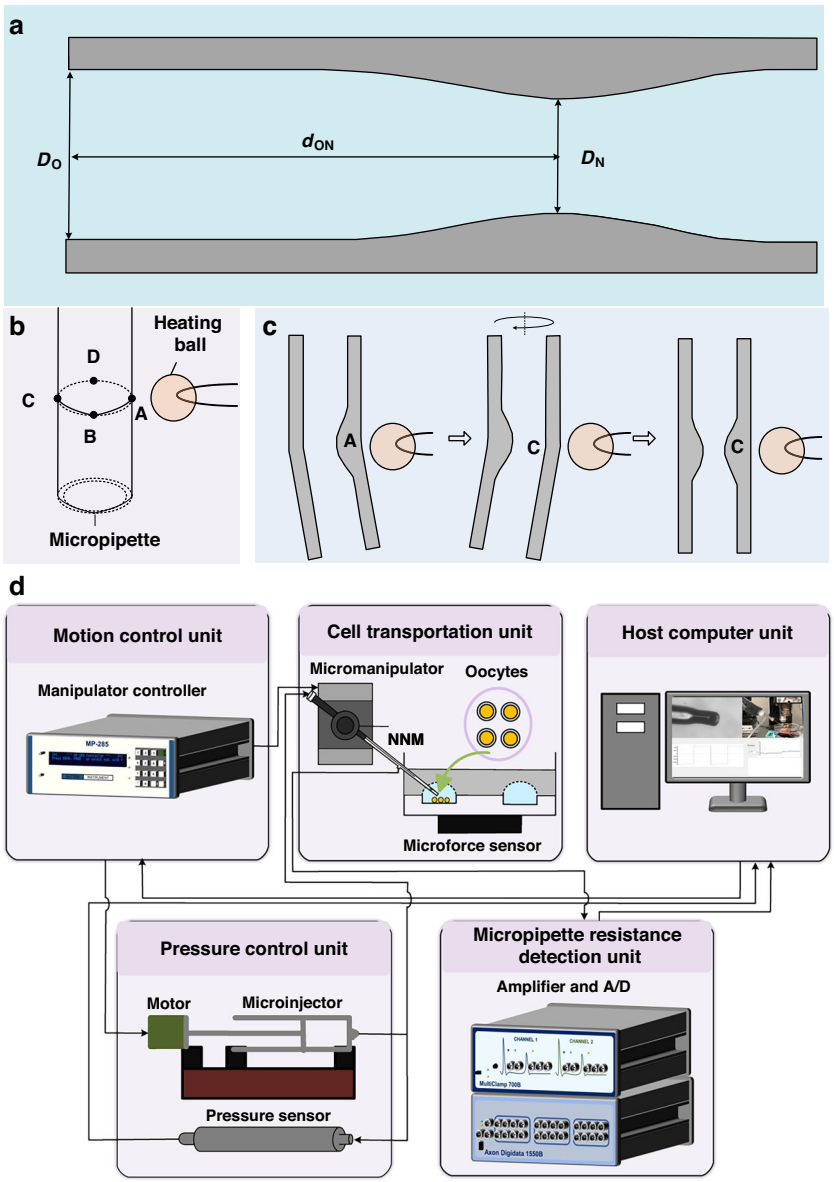

Fig. 2 The fabrication process of narrow-necked micropipette (NNM) and system setup of robotic cell transportation system. a Three key geometrical parameters of NNM, the inner radius at the micropipette opening D_O, inner radius at the narrow neck position D_N and the distance between the micropipette opening and narrow neck position d_{ON}. **b** The heating devices and four heating points to fabricate NNM from common straight micropipette. **c** The operation procedures of heating-and-rotating process to fabricate NNM. **d** Hardware device and information communication process in the robotic cell transportation system

cells and 100 μm-sized domestic oocytes are set as the 4-folded and 3-folded D_O, respectively.

Detailed methods for fabricating the NNMs for transportation of 10 μm-level and 100 μm-level sized cells are presented in Section 4 of the Supplementary file.

Robotic microscopic view-free cell transportation system setup

The proposed robotic cell transportation system is developed within our laboratory[21]. The system setup is shown in Fig. 2d. The proposed robotic cell transportation system consists of five units, namely the Motion control unit, Cell transportation unit, Pressure control unit, Micropipette resistance detection unit, and Host computer unit. The pressure control unit functions to provide and monitor the pressure inside the micropipette, and it is composed of a motor, an in-house developed microinjector[13,26,27] and a pressure sensor (PXM459-350HCG485-5V, OMEGA) with a resolution of 10 Pa. The specific functions of each unit of the robotic cell

transportation system are detailed in Section 6 of the Supplementary file.

Landing detection of micropipette tip based on gap resistance model

The measured impedance of the micropipette electrode after it enters the extracellular liquid and before it contacts any targets such as the cell or the petri dish bottom is termed bath impedance[28]. This section presents a landing detection method of the micropipette tip based on the gap resistance model. An electrical model of the micropipette landing process is established, analyzing resistance trends at the micropipette tip before and after landing. Real-time measurement of the liquid's electrical resistance enables automatic detection of electrically guided micropipette landing. The detailed content is presented in Section 7 of the Supplementary file. The liquid composition exerts a significant influence on the measurement results of micropipette resistance. The type and composition of the liquid are presented in Section 8 of the Supplementary file.

Aspiration and injection resistance modeling for cell holding and release detection

This section presents a method for cell holding and release detection based on aspiration and injection resistance modeling. The detailed content is presented in Section 9 of the Supplementary file.

Robotic cell transportation process without microscopic view

Based on the above work, a robotic visual cell transportation process is established as shown in Fig. S3. To save the paper length, the detailed introduction of the robotic cell transportation process and control diagram has been provided in Section 10 of the uploaded supplementary file "Supplementary file.pdf".

Results

A series of experiments are conducted in this section to validate the effectiveness of the proposed work in this paper. First, landing experiments of NNMs with different opening diameters were conducted to determine the size ranges of NNM openings suitable for gap resistance-based landing detection methods. Then holding and release experiments on NNMs with different narrow neck diameters were conducted to determine the inner diameter range suitable for micropipette resistance-based detection of cell holding and release. Further, robotic transportation experiments on HeLa cells and porcine oocytes were conducted to test the performance of our robotic transportation system on 10 μm-level sized and 100 μm-level sized cells. Finally, viability tests were conducted after transportation to evaluate the potential harm to cells.

Landing detection experiments based on micropipette resistance and based on contact force

Six NNMs with an inner opening diameter ranging from 10 μm to 60 μm with an interval of 10 μm. The inner diameter of the narrow neck of each micropipette is set as 0.6-folded opening diameter, which is close to the determined value in our previous study[21]. Each micropipette was mounted with a tilt angle of 45°. Each micropipette tip moves down to contact the petri dish bottom under the microscope at a constant speed of 10 μm/s. The landing experiments were conducted under microscope, with microscopic view to confirm the contact between the micropipette tip and petri dish bottom. When a horizontal motion of the micropipette tip is detected through the tip detection method in our previous research[22], which means the micropipette tip has touched the petri dish bottom, the recorded resistance of all micropipettes before and after the contact was plotted as shown in Fig. 3a.

It can be found that micropipette resistance basically remains constant at first because the micropipette resistance is too small to detect its variation when micropipette tip is still far away from the bottom, according to Eq. (16) in the Supplementary file. A significant rise in measured micropipette resistance occurs when the micropipette tip is close to the bottom before contacting it. It can be found from Fig. 3b that the above increase amplitudes reduce with the increase of opening diameter of the micropipette. When the diameter of the micropipette opening increases up to 50 μm, the above increase becomes too weak to be detected by our resistance recording system. After contact, the micropipette keeps moving downward and the measured micropipette resistance basically keeps constant or slight decrease when the micropipette opening diameter is larger than 50 μm. The above trend is in accordance with the analysis results in the section "Landing detection of micropipette tip based on gap resistance model".

In summary, the resistance variation measured by our system becomes too weak to be detected for landing detection when the micropipette diameter increases up to 50 μm. A new landing detection method is required for NNMs with an opening diameter larger than 50 μm.

To test the contact force of NNMs for 10 μm level-sized somatic cells, five of the above six NNMS with opening diameters varying from 10 μm to 50 μm with an interval of 10 μm were selected for the landing detection experiments through contact force. Besides, to test the contact force of NNMs for 100 μm level-sized domestic oocytes, NNMs with opening diameter varying from 50 μm to 800 μm with an interval of 100 μm were prepared for landing detection results.

Before micropipette landing on the petri dish bottom, the force sensor below the petri dish bottom is set to zero.

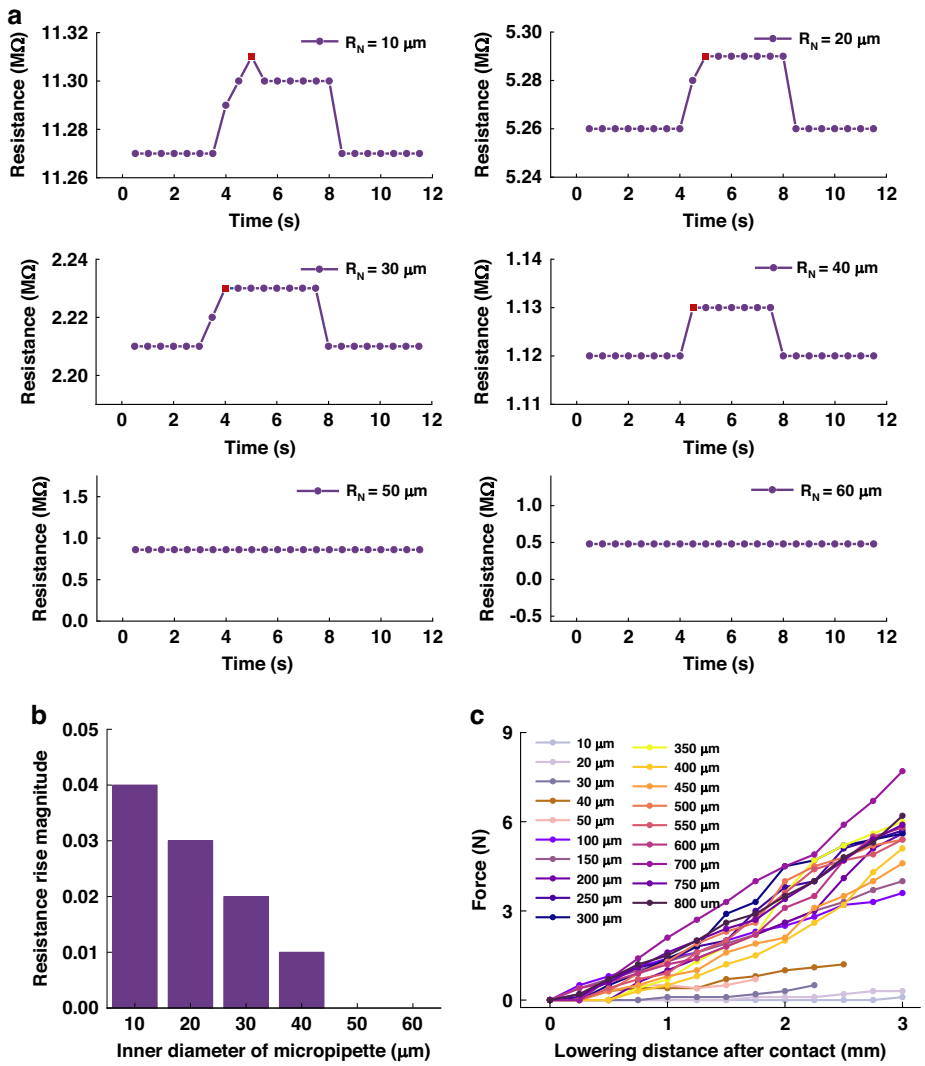

Fig. 3 Results of landing detection experiments of NNMS. a Resistance variation curves of micropipettes with different inner diameters during landing process. (The red square dots in the diagram indicate the contact points during the micropipette landing). **b** Increase in the magnitude of resistance during micropipette landing. **c** Contact force variation curves with respect to the further lowering distance after contact for micropipettes of different inner diameters

Then, after the micropipette tip contact is detected through horizontal motion of the micropipette tip, the detected force before and after the contact are plotted. The full results of all micropipettes are shown in Fig. 3c. It can be found that the contact force correlated positively with the opening diameter. When the opening diameter is less than 30 μm, the generated contact force after landing is too slight to be detected by our force sensor.

In summary, it can be found that for NNMs with an opening diameter larger than 50 μm, the contact force is a better indicator for landing detection. For the NNMs with an opening diameter of less than 30 μm, the micropipette resistance is a better indicator for landing detection. For the NNMs with an opening diameter between the above two threshold values, either of them can be utilized for landing detection.

Cell holding and release experiments of NNMs

To facilitate the blockage of NNM with different sizes, a series of NNMs with narrow necks fabricated at the opening are prepared for cell holding and release experiments. As the distance between the opening and narrow neck is only 3–4 folded cell diameter, which is far less than the length of the whole micropipette, the resistance of the liquid between the opening and narrow neck is far less than the whole liquid resistance inside NNMs R_{E2} in Eq. (13) in the Supplementary file, which can be ignored in the cell holding and release process. Thus,

when the narrow neck is fabricated at the opening of the micropipette, the detected resistance of the NNM can be treated as equal to a normal NNM with a narrow neck fabricated inside the micropipette, which means these NNMs can be utilized to test the proposed micropipette resistance-based cell holding and release method.

Five NNMs with inner diameter of narrow neck (which is also the micropipette opening) varying from 10 μm to 50 μm with an interval of 10 μm, and seven NNMs with inner diameter of narrow neck varying from 100 μm to 400 μm with an interval of 50 μm were prepared for the holding and release experiments. In the holding and release experiments, the NNMs with narrow neck sizes of 10 μm and 20 μm were utilized to hold and release the HeLa cells (with a diameter of 10-30 μm). The NNMs with narrow neck sizes varying from 30 μm and 100 μm were utilized to hold and release the porcine oocytes (with a diameter of about 150 μm). The NNMs with a narrow neck size larger than 100 μm were utilized to hold and release the zebrafish embryos (with a diameter of about 1 mm). The experiments were conducted under a microscope just for confirmation of the holding and release of the cell.

Figure 4 shows the resistance variation of NNMs during holding and release. It can be found that a sudden increase and decrease of the micropipette resistance were found for all micropipettes with different inner diameters of the narrow neck, which are in accordance with the analysis results in the section "Aspiration and injection resistance modeling for cell holding and release detection". The increase and decrease amplitudes of the micropipette resistance decrease as the increase of the inner diameter of narrow neck, as shown in Fig. 4b, c. This is mainly because of the following two reasons. First, the initial bath resistance of the micropipette decreases as the section area of the micropipette increases with the increase of the narrow neck size. Second, the quality of the seal between the cell membrane and narrow neck decreases as more gaps may be formed as the increase of contact area between the micropipette opening and cell surface, which reduces the top resistance value after cell holding.

In summary, all NNMs with an inner diameter of narrow neck from 10 μm to 400 μm show detectable increase and decrease of the micropipette during holding and release of the cell. Thus, the micropipette resistance of NNMs can be utilized for holding and release detection without a microscopic view.

Robotic transportation experiments on somatic cells and domestic oocytes

A total number of forty HeLa cells were prepared to validate the effectiveness of the proposed robotic transportation process for 10 μm level-sized somatic cells. The HeLa cells were prepared according to standard protocols given in Section 3.1 of the uploaded supplementary file "Supplementary file .pdf". Forty HeLa cells were randomly divided into two groups (twenty cells /group). The first group of cells was transported using the proposed methods in the section "Robotic cell transportation process without microscopic view". The microscopic view is provided not for transportation guidance but only for monitoring experimental processes and confirmation of experimental results. The second group of cells was transported by a common micropipette according to a previously developed automated transportation method based on microscopic view[13]. The operation process and detected micropipette resistance in landing, holding, and release are shown in Fig. 5a.

Eighteen of twenty HeLa cells were successfully transported from one pit to another through observation results in two pits after experiments, with a success rate of 90% (18/20). It is higher than the 55% (11/20) transfer success rate achieved by the conventional method. Meanwhile, this result is also higher than the 83.3% (25/30) transfer success rate achieved by the manual transportation method using NNM and the 53.3% (16/30) transfer success rate achieved by the previous robotic transportation method using CSM[29]. Experimental results of Hela cell transportation success rate with different methods are presented in Table 2. Through a recorded microscopic view of the operation process, two failures occur because they adhere to the micropipette surface during the searching process, leaving them to the previous droplet by the interface force between the previous droplet and the paraffin oil covering it when the micropipette leaves the previous droplet. For the eighteen cells which are successfully transported, the average operation time is 20.1±1.8s/cell ($n = 18$), which is faster than the manual microscopic view-based method using a common micropipette (28.3±3.3s/cell). For our method, about 63% of the time is spent in cell searching and moving from one droplet to another. For the cell positioning task, which is usually time-consuming for the traditional cell transportation task, the responding cell holding time in our operation, defined as the time from the moment micropipette resistance starts to increase to the moment it stops increasing, is only about 2 s according to Fig. 5a, which is faster than[13] is the shortest among related microscopic-view based method, which costs about 3 s on average for micro beads with similar size to HeLa cells in[13]. The above results demonstrate that our method can effectively reduce the cell positioning time in comparison to the traditional microscopic view-based method. This is mainly because the NNM can stop the cell by force with its narrow neck. The detailed robotic transportation of HeLa cells is provided in the uploaded supplementary file "Robotic transportation of HeLa cells .mp4".

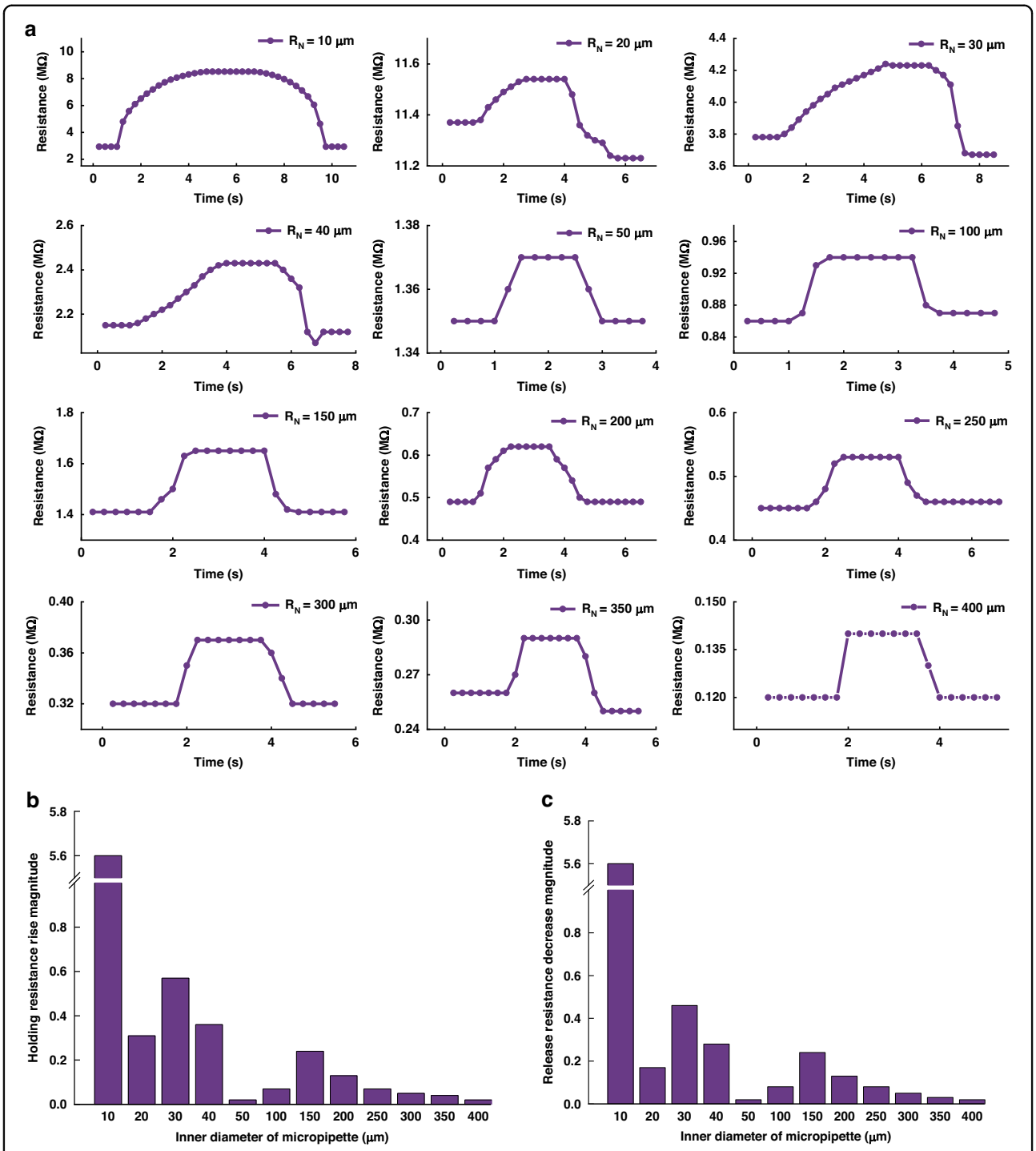

Fig. 4 Results of cell holding and release experiments of NNMs. a Resistance value changes in micropipettes with different inner diameters before and after aspiration and release. **b** The increase amplitudes of the micropipette resistance reduces as the increase of inner diameter of narrow neck. **c** The decrease amplitudes of the micropipette resistance reduces as the increase of inner diameter of narrow neck

A total of forty porcine oocytes were prepared to validate the effectiveness of the proposed robotic transportation process for 100 μm-level-sized domestic oocytes. The porcine oocytes were prepared according to standard protocols given in Section 3.2 of the Supplementary file. Forty porcine oocytes were randomly divided into two groups (twenty oocytes/group). The first group of cells was transported using the proposed methods in the

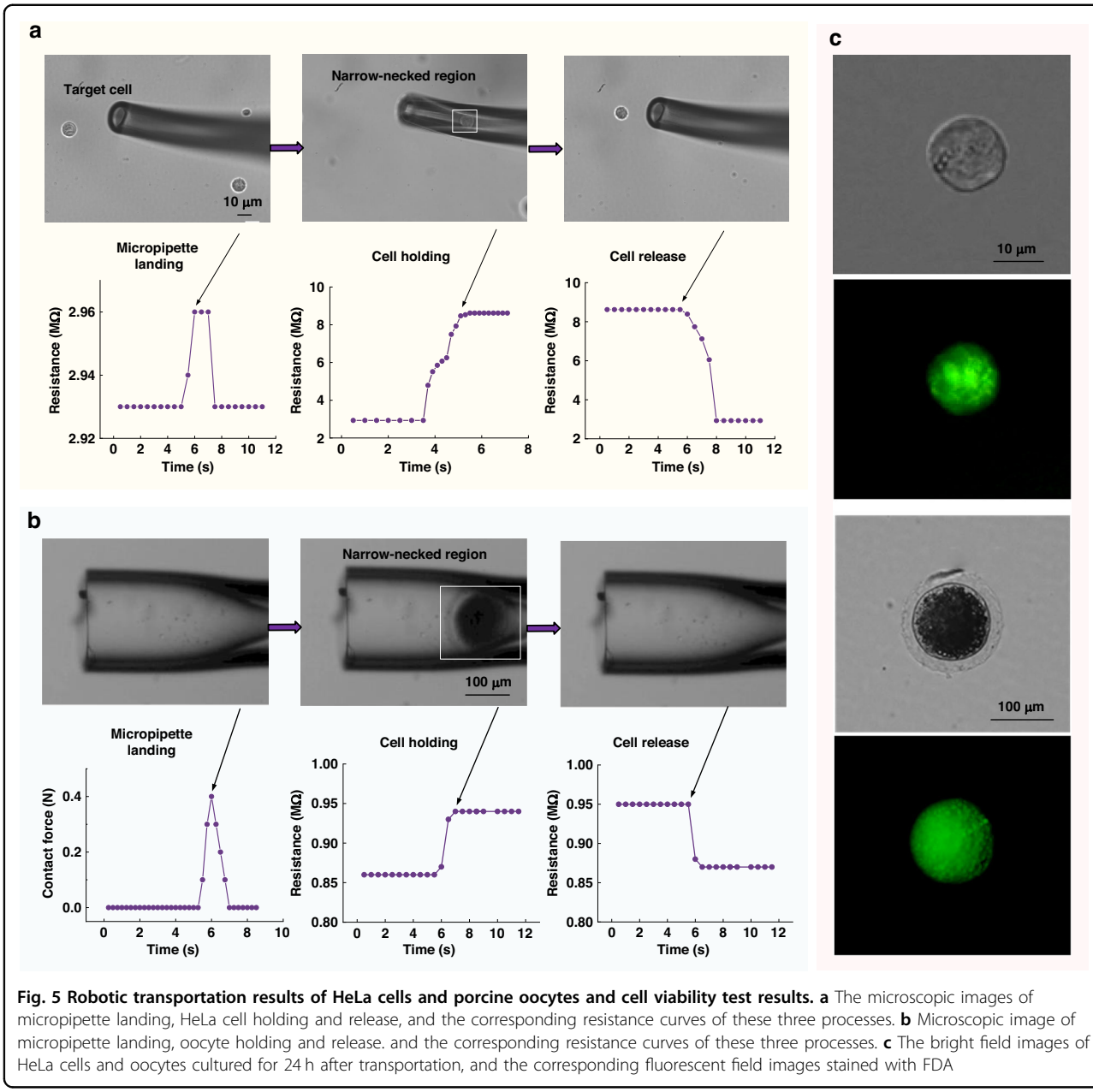

Fig. 5 Robotic transportation results of HeLa cells and porcine oocytes and cell viability test results. a The microscopic images of micropipette landing, HeLa cell holding and release, and the corresponding resistance curves of these three processes. **b** Microscopic image of micropipette landing, oocyte holding and release. and the corresponding resistance curves of these three processes. **c** The bright field images of HeLa cells and oocytes cultured for 24 h after transportation, and the corresponding fluorescent field images stained with FDA

Table 2 Experimental results of Hela cell transportation with different methods

Method	Cell transportation success rate	Average operation time
Robotic CSM[29]	53.3% (16/30)	–
Manual NNM	83.3% (25/30)	–
Conventional method[13]	55% (11/20)	28.3 ± 3.3 s/cell
Our method	90% (18/20)	20.1 ± 1.8 s/cell

section "Robotic cell transportation process without microscopic view". The second group of cells was transported by a common micropipette according to a previously developed automated transportation method based on microscopic view[13]. The transportation process and detected micropipette resistance and contact force in landing, holding and release are shown in Fig. 5b.

Nineteen of twenty oocytes were successfully transported from one pit to another through observation results in two pits after experiments, with a success rate of 95% (19/20). It is higher than the 80% (16/20) transfer success rate achieved by the conventional method. The

detailed robotic transportation of porcine oocytes is provided in the uploaded supplementary file "Robotic transportation of porcine oocyte .mp4". One failure occurs because two oocytes adhere to each other during cell picking, making one stay outside of the NNM opening and left in the previous droplet. For the nineteen cells that are successfully transported, the average operation time is 24.3 ± 5.2 s/cell (n = 19), which is comparable to the microscopic view-based methods (about 25 ± 3.1 s/cell). The cell positioning time is only about 1 s. This control time is faster than the results of porcine oocytes reported in ref. [13], which is about 3 s/cell, and totally comparable to the embryos positioning time of the linear quadratic regulator (LQR) controller in ref. [15] (about 1 s on average), which is fastest in microscopic view according to our knowledge.

Cell viability testing results

Ten HeLa cells and ten porcine oocytes operated by our robotic transportation method were cultured to evaluate the viability of these cells. In comparison, the same number of HeLa cells and porcine oocytes were transported by common straight micropipettes with a microscopic view, and the same number of cells not transported were also cultured to test their viabilities.

After 24 h culture, the HeLa cells and porcine oocytes were stained by the fluorescein diacetate (FDA) to observe whether the cells were still alive. The FDA fluorescent dye molecules can combine with active lipases in living cells and be hydrolyzed into fluorescent fluorescein, accumulating in the cells and emitting green fluorescence upon stimulation. The HeLa cells and porcine oocytes with green fluorescence are considered alive (see Fig. 5c). Else, they are treated as dead cells. The culturing results demonstrate that 9 of 10 HeLa cells and 10 of 10 porcine oocytes are alive after being operated on by our methods, showing 90% and 100% survival rates. In comparison, 100% (10/10) and 90% (9/10) survival rates of HeLa cells and porcine oocytes were achieved by a microscopic view-based method. For HeLa cells and porcine oocytes without transportation, the survival rates are all 100%.

The above results demonstrate that our microscopic-view-free method based on NNMs has a comparable survival rate in comparison to the traditional microscopic-view-based method using a traditional straight micropipette. This means our cell transportation method has limited harm to the cell survival rate.

Discussion

The common straight micropipette with a constant inner diameter lacks a structure inside the micropipette to stop the aspirated cell by force. Thus, the cell has to be positioned carefully by repeated adjustment of the aspiration pressure inside the micropipette. The above restrictions of common straight micropipettes limit their applications in cell transportation. This paper fabricated an NNM to hold the cell at the narrow neck position by force. Apparently, the cell holding can generate some cell deformation and mechanical stimulation to the target cell. Unfortunately, through setting an appropriate increase threshold of micropipette resistance to stop the aspiration, the generated cell deformation can be limited, which has been validated by the cell viability testing results in the section "Cell Viability Testing Results". Further, by setting an appropriate decrease threshold of micropipette resistance during cell release, the volume of liquid released to a new droplet can be limited to reduce the potential contamination problems.

At present, due to the power limitation of the microforge, the proposed heating and rotating fabrication method can only fabricate the NNMs with an opening diameter suitable for transporting 10-μm-level-sized somatic cells and 100-μm-sized domestic oocytes. For giant cells such as fish eggs, the bilayer micropipette made by inserting a thinner micropipette into a thick one can provide a large enough opening diameter for transporting the above giant oocytes. By equipping the bilayer micropipette, our system is expected to transport all cell types from 10-μm-level size to 1-mm-level size.

At present, the proposed gap resistance model can only detect the landing of a micropipette with an inclined angle. For the micropipette with the tip bent by a certain degree to let its tip be parallel with the horizontal plane, no gap resistance can be detected using our model. Fortunately, the above horizontal micropipette may not be suitable for a microscopic view-free cell transportation task because the horizontal tip of the micropipette may squeeze the target cell during the landing process. Thus, the gap resistance model is still suitable for landing detection for micropipette use in microscopic view-free transportation of cells.

The mechanical properties of the target cells, such as the cell stiffness and frictions on the cell surface, have significant influences on the resistance values detected during both holding and release processes. During cell holding, an excessively low Young's modulus can lead to excessive cell deformation under negative pressure, causing the cell to be completely aspirated into the micropipette. This not only prevents normal resistance signal measurement but also reduces the amplitude of the detected resistance variation, compromising the reliability of the cell holding detection. Further, the friction of the cell surface can also influence resistance measurements. If the friction between the cell surface and the narrow neck is large, the cell surface tends to adhere tightly to the inner wall of the narrow neck, significantly reducing the gap between them. According to Eq. (28) in the Supplementary file, this reduced gap increases the gap resistance

R_{EC2}, combined with Eq. (27) in the Supplementary file, the total resistance R_{EC} during cell holding correspondingly increases, making the rise in electrode resistance during holding more pronounced. Similarly, during cell release, the decrease in electrode resistance becomes more pronounced, facilitating both holding and release detection. Future work will systematically investigate the effects of these cellular mechanical properties and micropipette-cell interfacial friction characteristics on transportation performance to further improve the robustness and applicability of the system. In addition, the effects of environmental conditions such as temperature and humidity on the robotic transportation experiments have not been analyzed in detail. The temperature and humidity of the experimental environments will be adjusted in future studies to further explore their potential effects on the accuracy of electrical resistance measurements.

The quality of the seal between the micropipette and the target cell affects both holding and release-detection based on the resistance model. Specifically, Eq. (28) in the Supplementary file indicates that if the cell adheres tightly to the inner wall of the micropipette with a good seal, the gap between them will be significantly reduced, thereby increasing the gap resistance R_{EC2}. Combined with Eq. (27) in the Supplementary file, during cell holding, the total resistance increases correspondingly, resulting in a more apparent rise in the micropipette electrode resistance. Similarly, when the seal between the micropipette inner surface and the target cell is strong, the decrease in electrode resistance during release becomes more pronounced, facilitating timely and accurate detection of release events. Conversely, if the seal between the cell and the micropipette wall is insufficiently tight, resulting in a larger gap, the resistance changes during both cell holding and release are reduced, which increases the difficulty of achieving reliable detection based on resistance variations. Therefore, good sealing quality is an important condition for ensuring the sensitivity and reliability of the holding and release detection method in this manuscript.

To enhance operational efficiency, the following optimization strategies can be implemented in the future: first, multiple target cells can be stored in a thick micropipette prior to the experiment and injected out of the storage micropipette one by one in cell transportation, thereby reducing the time spent on searching for target cells within droplets and accelerating the whole transfer speed. Second, the distance between droplets can be optimized to shorten the distance between the source droplet and the target droplet, further improving the execution efficiency of the transportation system. To enhance cell transfer success rates, utilizing higher-sensitivity microforce sensors to accurately detect minimal contact forces can improve the detection accuracy of micropipette tip landing on the bottom of the peri dish, reducing operational errors, and thereby increasing the success rate of the cell transportation. Besides selecting amplifiers with superior performance to enhance the sensitivity of the resistance detection system enables the system to accurately capture minute resistance changes during cell holding and release, thereby further improving system stability and transportation success rates.

At present, our system still uses traditional cell operation tools such as micropipettes to transport cells, which makes it hard to form a parallel system due to the limited number of micropipette holding devices. As the resistance detection and pressure control can be realized through microfluidic devices fabricated by micro-electro-mechanical systems (MEMS) technique, our system can be upgraded to a parallel version to improve the operation through put in the future. With the small size of the whole microfluidic system, the future version is highly expected to be utilized in the full in-box cell culturing and operation system in the future.

Conclusion

This paper proposed a robotic cell transportation system to transport common-sized somatic cells and oocytes without microscopic view. A narrow-necked micropipette (NNM) was fabricated to hold and release the cell inside the micropipette during transportation. A gap resistance model, an aspiration and injection resistance model of the NNM were developed for landing on the petri dish bottom, holding, and releasing the cell without microscopic view feedback. Based on the above work, a robotic resistance-guided transportation process was developed for transporting common-sized cells without a microscopic view. Experimental results demonstrate that the proposed system can land on the petri dish bottom with 100% success rate. It can transport 10-μm-level-sized HeLa cells and 100-μm-level-sized porcine oocytes with efficiencies comparable to common microscopic view-based methods. The culture results and viability testing results demonstrate no harm to the cell survival rate. Our microscopic cell transportation system can be easily upgraded to a microfluidic version, which is able to perform high-throughput cell transportation for integrated and automated cell engineering applications in the future.

Acknowledgements

This research was supported in part by the National Natural Science Foundation of China under Grant 62273186 and Guangdong Basic and Applied Basic Research Foundation under Grant 2024A1515011171, and Shenzhen Science and Technology Program under Grant JCYJ20250604185817023, and in part by the Beijing Advanced Innovation Center for Intelligent Robots and Systems under Grant 2019IRS05.

Author contributions

Q.Zh. wrote the manuscript, prepared the figures, designed and guided experiments. M.L., R.Zh., and J.Q. conducted the experiments and revised the

manuscript. Sh.Fu. and R.L. checked the manuscript. X.Zh. guided the research, revised the manuscript, and checked it for final submission.

Data availability
The data that support the findings of this study are available from the corresponding author upon reasonable request.

Conflict of interest
The authors declare no competing interests.

Ethics approval and consent to participate
All experiments in the present study were conducted in accordance with the Regulations on the Administration of Laboratory Animals (Ministry of Science and Technology of China). All procedures in the present study were approved by the Laboratory Animal Center Ethics Committee of Nankai University, Tianjin, China (approval number SYXK (Tianjin) 2024- 0013).

Supplementary information The online version contains supplementary material available at https://doi.org/10.1038/s41378-026-01193-5.

Received: 20 October 2025 Revised: 16 December 2025 Accepted: 23 December 2025
Published online: 27 February 2026

References

1. Zhang, Y., Li, B., Liu, Y. & Zhao, X. Modeling and tracking control of micropipette oocyte enucleation based on fractional calculus. *IEEE Trans. Ind. Electron.* **72**, 11791–11800 (2025).
2. Xie, P., Tsai, S., Rosenwaks, Z. & Palermo, G. D. A new approach to promote cell fusion in nuclear transplantation aiming at neogametogenesis. *Fertil. Steril.* **122**, e364 (2024).
3. Miao, S. et al. Microfluidics-enabled robotic system for embryo vitrification with real-time observation: design, method, and evaluation. *IEEE/ASME Trans. Mechatron.* **29**, 179–189 (2023).
4. Lin, H. et al. Development of an automated device for the optimization of oocyte and embryo vitrification. *Cryobiology* **120**, 105275 (2025).
5. Casciani, V., Galliano, D., Franasiak, J. M., Mariani, G. & Meseguer, M. Are we approaching automated assisted reproductive technology? Embryo culture, metabolomics, and cryopreservation. *FS Rev.* **2**, 251–264 (2021).
6. Liu, M. et al. Robotic improved micropipette aspiration method for accurate measurement of cellular mechanical properties. *IEEE Trans. Instrum. Meas.* **74**, 1–8 (2025).
7. Peng, X., Urso, M., Ussia, M. & Pumera, M. Shape-controlled self-assembly of light-powered microrobots into ordered microchains for cells transport and water remediation. *ACS Nano* **16**, 7615–7625 (2022).
8. Fuchs, S. et al. In-line analysis of organ-on-chip systems with sensors: integration, fabrication, challenges, and potential. *ACS Biomater. Sci. Eng.* **7**, 2926–2948 (2021).
9. Shan, G. et al. Model-based robotic cell aspiration: tackling nonlinear dynamics and varying cell sizes. *IEEE Robot. Autom. Lett.* **5**, 173 (2019).
10. Kong, S. et al. Photobleaching-induced changes in the optical and photochemical properties of algal organic matter. *Water Res.* **243**, 120395 (2023).
11. Moud, A. A. Fluorescence recovery after photobleaching in colloidal science: introduction and application. *ACS Biomater. Sci. Eng.* **8**, 1028–1048 (2022).
12. Zhang, X. et al. Controlled aspiration and positioning of biological cells in a micropipette. *IEEE Trans. Biomed. Eng.* **59**, 1032–1040 (2012).
13. Zhao, X. et al. Aspirating cell into orifice of micropipette for precise cell transportation using micropipette. *IEEE Trans. Autom. Sci. Eng.* **21**, 181–191 (2022).
14. Sun, M. et al. Precise aspiration and positioning control based on dynamic model inside and outside the micropipette. *IEEE Trans. Autom. Sci. Eng.* **20**, 385–393 (2022).
15. Zhang, Z. et al. Robotic pick-and-place of multiple embryos for vitrification. *IEEE Robot. Autom. Lett.* **2**, 570–576 (2016).
16. Miao, S. et al. A robotic system with embedded open microfluidic chip for automatic embryo vitrification. *IEEE Trans. Biomed. Eng.* **69**, 3562–3571 (2022).
17. Arav, A. et al. A new, simple, automatic vitrification device: preliminary results with murine and bovine oocytes and embryos. *J. Assist. Reprod. Genet.* **35**, 1161–1168 (2018).
18. Roy, T. K. et al. Embryo vitrification using a novel semi-automated closed system yields in vitro outcomes equivalent to the manual Cryotop method. *Hum. Reprod.* **29**, 2431–2438 (2014).
19. Shojaei-Baghini, E., Zheng, Y. & Sun, Y. Automated micropipette aspiration of single cells. *Ann. Biomed. Eng.* **41**, 1208–1216 (2013).
20. Wang, T. Y., Libardo, M. D. J., Angeles-Boza, A. M. & Pellois, J. P. Membrane oxidation in cell delivery and cell killing applications. *ACS Chem. Biol.* **12**, 1170–1182 (2017).
21. Qiu, J. et al. Robotic microscopic vision-free cell transportation based on pressure variation model inside bilayer micropipette. *IEEE Trans. Autom. Sci. Eng.* **22**, 4134–4144 (2024).
22. Zhao, Q. et al. Robotic patch clamp based on noninvasive 3-d cell morphology measurement for higher success rate. *IEEE Trans. Instrum. Meas.* **71**, 1–12 (2022).
23. Wang, W. H., Liu, X. Y. & Sun, Y. Contact detection in microrobotic manipulation. *Int. J. Robot. Res.* **26**, 821–828 (2007).
24. González-Bermúdez, B., Guinea, G. V. & Plaza, G. R. Advances in micropipette aspiration: applications in cell biomechanics, models, and extended studies. *Biophys. J.* **116**, 587–594 (2019).
25. Maxime, B. et al. A deep learning strategy to identify cell types across species from high-density extracellular recordings. *Cell* **188**, 2218–2234 (2025).
26. Guo, X. et al. Design and developing a robot-assisted cell batch microinjection system for zebrafish embryo. *Microsyst. Nanoeng.* **11**, 29 (2025).
27. Guo, Z., Ai, N., Ge, W. & Xu, Q. Design of an automated robotic microinjection system for batch injection of zebrafish embryos and larvae. *Microsyst. Nanoeng.* **10**, 20 (2024).
28. Gray, M. & Santin, J. M. Series resistance errors in whole cell voltage clamp measured directly with dual patch-clamp recordings: not as bad as you think. *J. Neurophysiol.* **129**, 1177–1190 (2023).
29. Shan, G. et al. Model-based robotic cell aspiration: tackling nonlinear dynamics and varying cell sizes. *IEEE Robot. Autom. Lett.* **5**, 173–178 (2019).